REPORT

WATER THERMODYNAMICS

Maxima in the thermodynamic response and correlation functions of deeply supercooled water

Kyung Hwan Kim,[1]* Alexander Späh,[1]* Harshad Pathak,[1] Fivos Perakis,[1] Daniel Mariedahl,[1] Katrin Amann-Winkel,[1] Jonas A. Sellberg,[2] Jae Hyuk Lee,[3] Sangsoo Kim,[3] Jaehyun Park,[3] Ki Hyun Nam,[3] Tetsuo Katayama,[4] Anders Nilsson[1]†

Femtosecond x-ray laser pulses were used to probe micrometer-sized water droplets that were cooled down to 227 kelvin in vacuum. Isothermal compressibility and correlation length were extracted from x-ray scattering at the low–momentum transfer region. The temperature dependence of these thermodynamic response and correlation functions shows maxima at 229 kelvin for water and 233 kelvin for heavy water. In addition, we observed that the liquids undergo the fastest growth of tetrahedral structures at similar temperatures. These observations point to the existence of a Widom line, defined as the locus of maximum correlation length emanating from a critical point at positive pressures in the deeply supercooled regime. The difference in the maximum value of the isothermal compressibility between the two isotopes shows the importance of nuclear quantum effects.

Water has remarkable physical properties that differ from almost all other liquids. In the ambient temperature regime, the properties of water already deviate from those of a simple liquid, and this deviation is strongly enhanced upon supercooling (*1*). In particular, the finding that the thermodynamic response and correlation functions—such as the isothermal compressibility (κ_T), heat capacity (C_P), thermal expansion coefficient (α_P), and correlation length (ξ)—appear to diverge toward a singular temperature (T_s), estimated by power-law fits of about 228 K at 1 bar (*2*, *3*), has led to several hypotheses about the origin of water's anomalous properties (*4*, *5*). The challenge is that the temperature T_s lies in a region of the phase diagram that has been denoted as "no man's land," because the kinetically controlled ice crystallization occurs on a much faster time scale than the experimentally accessible time scale in a typical laboratory setting. Because of this experimental constraint, the response functions have so far only been accurately measured in bulk water 10 to 20 K above the estimated T_s (*2*, *3*, *6*), making it impossible to distinguish between the proposed hypotheses describing the behavior of water in the deeply supercooled regime (*4*).

One hypothesis to explain the apparent divergence is that there exists a liquid-liquid transition with a liquid-liquid critical point (LLCP) at rather high positive pressures (*7*, *8*) or very close to ambient pressure (*9*). In this scenario, the Widom line, defined as the locus of correlation length maxima in the pressure-temperature (*P-T*) plane, emanates from the LLCP as a continuation of the liquid-liquid transition line into the one-phase region (*10*). The other thermodynamic response functions are also expected to have maxima near the Widom line. Another scenario brought forth to explain the diverging properties is the singularity-free model (*11*), which assumes a continuous transformation without discontinuity and with maxima of the response functions not only at ambient pressures but at all pressures. Alternatively, according to the critical point–free model, the LLCP is expected to occur at negative pressure (*12*), in which case the liquid-liquid phase transition would occur at T_s and the coexistence of two phases would be observed (*13*). Finally, it has also been proposed that ice crystallization occurs on a faster time scale than liquid equilibration, causing fluctuations into local structures that are similar to ice nuclei (*14*, *15*). These scenarios do not agree, and, to date, convincing experimental data of supercooled bulk water are still lacking.

Here we demonstrate that the thermodynamic response and correlation functions can experimentally be extracted down to 227.7 ± 1 K at ≈0 bar from x-ray scattering measurements in the low– and intermediate–momentum transfer (q) region of micrometer-sized water droplets using the x-ray lasers Pohang Accelerator Laboratory–X-Ray Free-Electron Laser (PAL-XFEL) in Korea and SPring-8 Angstrom Compact Free-Electron Laser (SACLA) in Japan. In particular, by analyzing the structure factor at low-q values, we determine the κ_T and ξ. Both of these properties show maxima as a function of temperature that coincide closely with the temperature of maximum increase in tetrahedral structures, as extracted by analysis of the structure factor at the first diffraction peak. These observations provide direct evidence for the existence of a Widom line in supercooled water and strongly support the LLCP scenario. The data also show that the κ_T maximum is higher for H_2O than for D_2O, demonstrating the importance of nuclear quantum

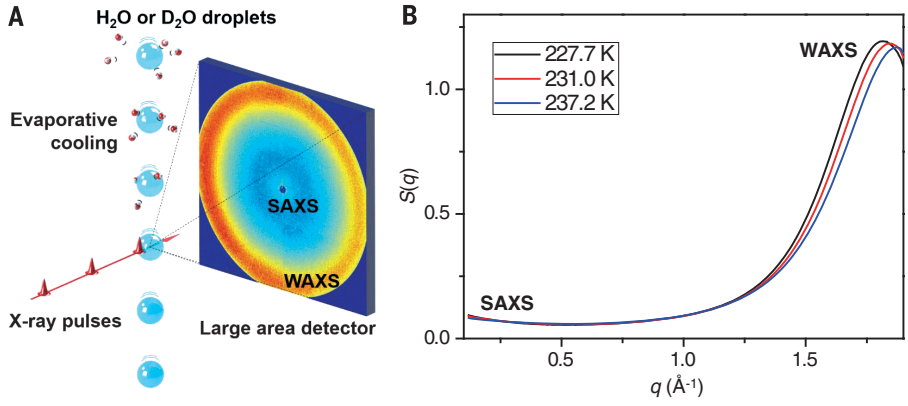

Fig. 1. Single-shot x-ray scattering of supercooled H_2O and D_2O under evaporative cooling conditions at the PAL-XFEL facility. (**A**) Schematic diagram of the experimental setup. A continuous series of droplets, each with a uniform diameter of ~14 μm, was generated by a droplet dispenser in vacuum, and the scattering patterns were generated by x-ray pulses with a photon energy of 5.5 keV. Various temperature points were measured by changing the distance between the dispenser and the measurement point. (**B**) Temperature-dependent scattering structure factor of H_2O. The wide dynamic range of the detector (MX225-HS, Rayonix) allows us to simultaneously measure the SAXS and WAXS regions for each x-ray shot. Data from three different temperature points (227.7, 231.0, and 237.2 K) are shown as examples.

[1]Department of Physics, AlbaNova University Center, Stockholm University, SE-10691 Stockholm, Sweden. [2]Biomedical and X-Ray Physics, Department of Applied Physics, AlbaNova University Center, KTH Royal Institute of Technology, SE-10691 Stockholm, Sweden. [3]Pohang Accelerator Laboratory, Pohang, Gyeongbuk 37673, Republic of Korea. [4]Japan Synchrotron Radiation Research Institute, Kouto 1-1-1, Sayo, Hyogo 679-5198, Japan.
*These authors contributed equally to this work.
†Corresponding author. Email: andersn@fysik.su.se

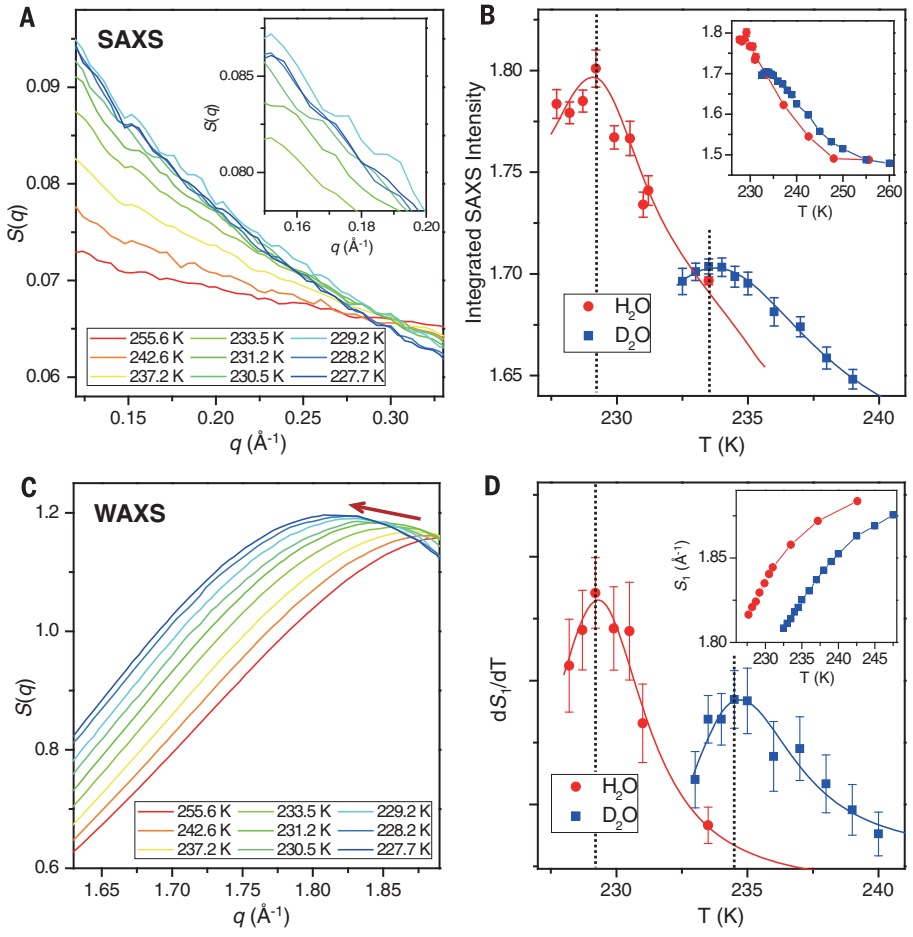

Fig. 2. SAXS and WAXS. (**A**) Temperature-dependent $S(q)$ of H_2O at the SAXS region. The SAXS intensity initially increases upon cooling, reaches the maximum at around 229 K, and then subsequently decreases at lower temperatures. The inset shows the magnified view from q = 0.15 to 0.2 Å^{-1}. (**B**) Integrated SAXS intensity from q = 0.12 to 0.2 Å^{-1} for H_2O (red circle) and D_2O (blue square), which shows maxima at around 229 and 234 K, respectively. Solid red and blue lines are shown to guide the eye. Dotted black lines indicate the position of the maximum. (**C**) Temperature-dependent $S(q)$ of H_2O around the WAXS region. With decreasing temperature, the position of the peak (S_1) is continuously shifting toward lower-q values (indicated by red arrow) as a result of increasing tetrahedrality of water. (**D**) Temperature dependence of S_1 varying around q = 1.85 Å^{-1} (inset) and its temperature derivative calculated numerically, dS_1/dT (main panel). Solid red and blue lines are shown to guide the eye. Dotted black lines indicate the position of the maximum. Note that in all figures the absolute temperature error bar is ±1 K, and the relative temperature error bar between data points is negligible on the scale of the x axis.

effects to partly explain the unusual properties of water.

Figure 1A shows a schematic of the experiment (*16*) performed at PAL-XFEL, where micrometer-sized water droplets (diameter 14 μm) undergoing evaporative cooling at ≈0 bar were probed with ultrafast x-ray scattering (pulse duration <50 fs, photon energy 5.5 keV). The droplet temperature was varied by adjusting the distance between the dispenser nozzle and the x-ray pulse interaction region, effectively changing the cooling-time duration (*17*). The temperature determination was performed by using a ballistic evaporation model (*16*), which has been tested by molecular dynamic simulations (*18*) and previously calibrated by measurements taken from in the deeply supercooled region (*17*). The large-area detector used at PAL-XFEL has the capability to cover an extended q range and thereby simultaneously record the wide-angle x-ray scattering (WAXS) region near the first diffraction peak and the small-angle x-ray scattering (SAXS) region, which is sensitive to density fluctuations.

At PAL-XFEL, we obtained reliable data down to 0.12 Å^{-1} where the cutoff was given by the edge scattering of the droplets, whereas the smaller x-ray focus at SACLA allowed measurements down to 0.08 Å^{-1} but was limited to temperatures down to 231.4 ± 1 K. The WAXS region of the data is essential to obtain a proper normalization of the structure factor in absolute units (*16*). Furthermore, the use of an x-ray laser also allowed the detection of potential Bragg peaks from crystalline ice on a single-shot basis, allowing us to separate the shots that were probing pure water from those containing small ice crystals (*17*). In this way, we obtained pure water shots for H_2O and D_2O down to 227.7 ± 1 and 232.5 ± 1 K, respectively; at lower temperatures, only ice shots were observed.

Figure 1B shows the structure factor [$S(q)$] obtained from the scattering patterns (*16*) for three different water temperatures, where we observed the shift of the first diffraction peak position around q = 1.75 Å^{-1} (WAXS) and the enhancement in the low-q region, below q = 0.5 Å^{-1} (SAXS). These findings demonstrate that, for each x-ray shot, we could simultaneously detect the structural changes in the WAXS region, related to the growth of tetrahedral structures (*17*), and the enhancement in the SAXS region, where the isothermal compressibility and the correlation length could be extracted. In this way, we experimentally provide a direct connection between the thermodynamic response functions and structural changes upon supercooling into the no man's land of the phase diagram.

Figure 2A shows the structure factor of H_2O in the low-q SAXS region averaged at a given temperature. In the low-q region, the structure factor increased upon cooling; the lowest temperatures are detailed in the inset. Note that the highest curve was not observed for the lowest temperature at 227.7 ± 1 K but rather for 229.2 ± 1 K, indicating that a maximum has been reached upon cooling. Figure 2B shows the integrated structure factor between 0.12 and 0.20 Å^{-1} for both H_2O and D_2O data, where we observed a maximum in the integrated low-q structure factor at 229.2 ± 1 K for H_2O and 233.7 ± 1 K for D_2O. The integrated structure factor at the maxima was higher for H_2O than for D_2O.

Figure 2C shows the first peak in the structure factor of water, where a continuous shift was seen to lower-q values with decreasing temperature, in agreement with previous work demonstrating growth of tetrahedral structures (*17*, *19*). The inset of Fig. 2D shows the peak position (*16*) as a function of temperature, where we note that the slope became steeper below 240 K (*4*). After the change in slope was quantified, the derivative of the peak position with respect to temperature (Fig. 2D) indicated the temperature at which the liquid underwent the most rapid increase toward tetrahedral coordination (*17*), and a maximum was seen for both H_2O and D_2O at 229.2 ± 1 and 234.5 ± 1 K, respectively. Notably, both quantities obtained from the structure factor in the SAXS (Fig. 2B) and WAXS (Fig. 2D) regions exhibited maxima in the same temperature range. Additionally, this trend was confirmed for both isotopes. Furthermore, both the integrated structure factor and the structure temperature-dependent derivative at the maxima were higher for H_2O than for D_2O.

The κ_T is thermodynamically linked to the structure factor S at q = 0 by the relation

$$S(0) = k_B T n \kappa_T \quad (1)$$

where k_B is the Boltzmann constant, T is the absolute temperature, and n is the molecular number density (*20*). It has been shown that κ_T

extracted from the low-q region closely follows thermodynamic measurements (*2*). To extract κ_T and ξ from the experimental data, we made use of Ornstein-Zernike (OZ) theory to describe the anomalous fluctuations in the liquid from SAXS data (*2*, *16*). Here we decompose the experimental $S(q)$ into two contributions: the S_{ref} following a simple liquid behavior, as seen, for instance, in ethanol (*21*), monotonically increasing with q in the relevant range and the S_{AN} for the anomalous excess scattering at low q (*2*). The S_{ref} is represented in the framework of the Percus-Yevick approximation for a hard-sphere fluid (*16*), and S_{AN} is described in OZ theory by a Lorentzian

$$S_{OZ} \propto 1/(\xi^{-2} + q^2) \quad (2)$$

where ξ is the OZ correlation length related in real space to the damping factor in the asymptotic decay of the pair-correlation function of the system (*22*). Figure 3A shows the results obtained from following the same procedure as in (*2*) to decompose $S(q)$ into the S_{ref} and the S_{AN} components. The S_{AN} was then fitted by using Eq. 2 to obtain S_{OZ} and thereby deriving ξ (*16*). To obtain the fitted $S(q)$, we added S_{OZ} and S_{ref}, as shown in Fig. 3A, indicating a good fit to the experimental data. For temperatures above 231.4 ± 1 K, this procedure was further tested by extension to lower-q values by using the SACLA data (*16*). From the fitted $S(q)$, we extracted the $S(0)$, which was used in Eq. 1 along with the experimental value of the density extrapolated into the no man's land (*16*), to derive the κ_T.

Figure 3B shows ξ in H_2O as a function of temperature with a maximum at 229.2 ± 1 K followed by a decrease at lower temperatures. For D_2O, the maximum is seen at 233.0 ± 1 K, but here only one data point could be observed at lower temperatures. The Widom line is defined as the locus of points in the P-T surface, which had a maximum in ξ. The observed maxima were thus direct evidence for the existence of such a line in supercooled water. Both isotopes gave a similar value of ξ with a maximum of around 4 Å, whereas the temperature dependence was stronger for D_2O than for H_2O. To assign ξ to an average fluctuation length scale at the Widom line, we assumed a spherical shape with the diameter $d \approx 4.5\xi$ (*23*), which corresponds to roughly 2 nm or around 130 molecules. Note that many fluctuating regions will be both smaller and larger than this average.

Figure 3C shows the variation of κ_T as a function of temperature. Maxima were observed at 229.2 ± 1 and 233.0 ± 1 K for H_2O and D_2O, respectively. Because the area in the low-q region of the structure factor shown in Fig. 2B was first-order proportional to the $S(0)$ (*16*), we expected a similar trend in the κ_T temperature dependence with the additional correction for number density and temperature in Eq. 1. We note that the maximum in κ_T is located at temperatures very close to the original power law–fit estimation T_s for the two isotopes (*24*). In this case, instead of divergence toward infinity, we observed finite maxima in κ_T and ξ. Another important observation is that κ_T at its maximum was at a higher value for H_2O than for D_2O.

The observation of maxima in two of the thermodynamic response and correlation functions, i.e., in κ_T and ξ at temperatures near where the liquid was undergoing the most rapid structural change with temperatures, is fully consistent with the concept of the Widom line in the LLCP scenario. We can rule out that the appearance of the maxima was caused by the structural arrest of the liquid, falling out of equilibrium as a result of nearing a temperature at which a high rate of ice formation occurs (*14*, *15*), as this would imply that the liquid structure (i.e., the shift observed in the WAXS) would stop changing with temperature, contrary to our observation of a distinct and accelerated shift. Furthermore, simulations that showed rapid ice crystallization exhibited only a modest increase in κ_T (*25*), far from the high maximum observed experimentally.

The continuous change of the structure factor (Fig. 2C) is not consistent with a liquid-liquid transition at ambient pressure, as suggested by the critical point–free model. In that case, we would instead expect a discontinuous change with the coexistence of two peaks in the structure factor, recently seen at extremely low temperatures above the glass transition where such a transition occurs (*13*). This finding is aligned with the conclusion obtained from recent measurements of interfacial ice growth in this temperature regime, indicating that the diffusion coefficient of the liquid shows no sign of an abrupt change associated with a phase transition (*26*). The presence of maxima in the thermodynamic and correlation response functions would also be consistent with the singularity-free model. However, in microscopic models, the singularity-free behavior arises only in the artificial limit in which a molecule's

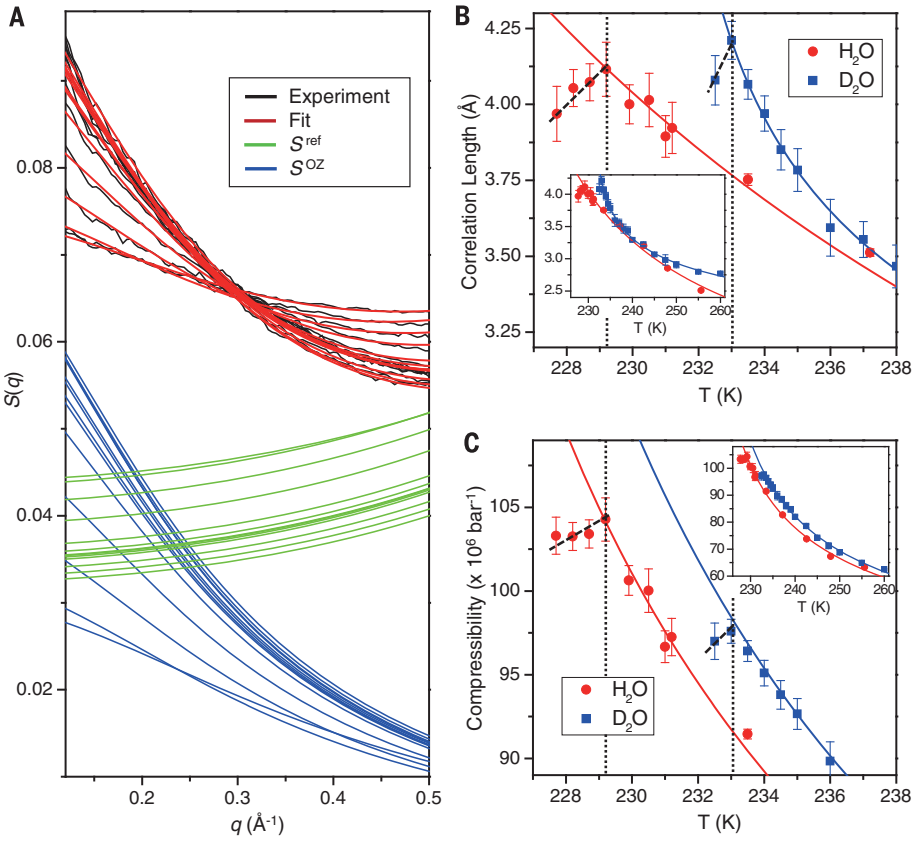

Fig. 3. Correlation length and isothermal compressibility. (**A**) OZ analysis of SAXS curves of H_2O. The experimental structure factor (black) was decomposed into a normal liquid contribution S_{ref} (green) and an anomalous excess OZ contribution S_{OZ} (blue) by using the fitting procedures described in the supplementary materials. (**B**) Temperature-dependent OZ correlation length ξ of H_2O (red) and D_2O (blue) determined from Eq. 2. A power-law fit (solid red and blue lines) is used to guide the eye to the maxima and is followed by a dashed black line to indicate the change in direction of the slope. Dotted black lines indicate the position of the maximum. (**C**) Temperature-dependent κ_T of H_2O (red) and D_2O (blue) obtained from the extrapolation to the zero momentum transfer [S(0)] and by using Eq. 1. A power-law fit (solid red and blue lines) is used to guide the eye to the maxima and is followed by a dashed black line to indicate the change in direction of the slope. Dotted black lines indicate the position of the maximum. Note that in all figures the absolute temperature error bar is ±1 K, and the relative temperature error bar between data points is negligible on the scale of the x axis.

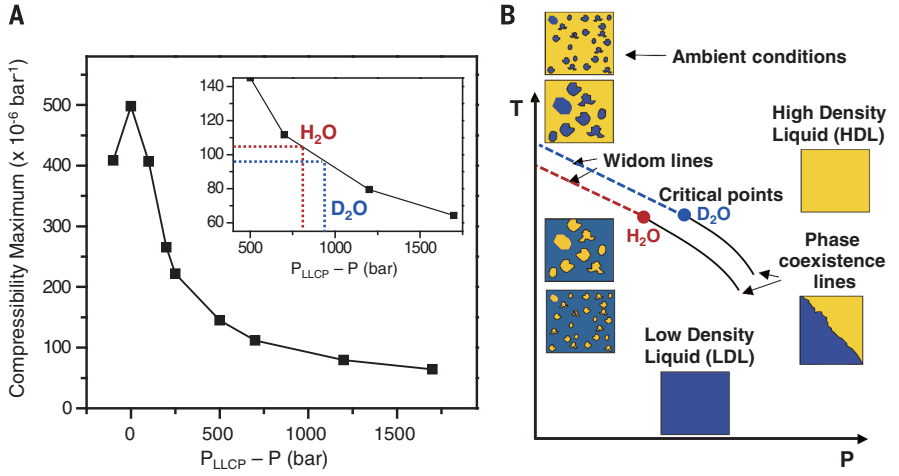

Fig. 4. Connection to the LLCP. (**A**) The maximum of the compressibility as a function of the pressure difference compared to the LLCP estimated by MD simulations performed with the iAMOEBA water model. The inset shows a magnified view from 450 to 1750 bar. H_2O and D_2O have compressibility maxima of ~105 × 10^{-6} and ~95 × 10^{-6} bar^{-1}, which correspond to pressure differences with respect to the LLCP of ~800 and ~950 bar, respectively. (**B**) Schematic picture of a hypothetical phase diagram of liquid water, showing the Widom lines with the inflection point of population conversion and maxima in length scale of fluctuations involving high- and low-density liquids together with the estimated relative positions of the LLCP for H_2O and D_2O.

hydrogen-bonding connectivity is completely uncorrelated (*11*, *27*), making it less consistent with a rapid increase in tetrahedral structures that grow to large sizes at the maxima. Furthermore, because this model implies a continuous transition at all pressures and temperatures, it is particularly inconsistent with the observation of interconverting peaks in the structure factor at low temperatures above the glass transitions, where diffusion is occurring, indicative of a discontinuous transition between liquid states (*13*). These observations only show consistency with the LLCP model.

Figure 4A shows a rough estimate of a potential location of the LLCP in the phase diagram based on the variation of the maxima along isobars of κ_T (*25*) using the iAMOEBA model (*28*). The model shows that the maxima increase with pressure up to 1700 bar where κ_T reaches an extremely high value (*25*). Although no true criticality could be observed, because of limitations in the size and time scale of the simulation together with coarsely spaced data points, we infer that this region of the phase diagram is in the neighborhood of a LLCP. The inset in Fig. 4A shows that the experimental values at ambient pressure of the maxima in κ_T would indicate that the LLCP is located around 800 bar for H_2O and 950 bar for D_2O. For consistency, we note that simulations with the WAIL method gave a LLCP at 400 to 500 bar (*29*), which is much closer to ambient pressure than the current LLCP estimate, explaining the observed κ_T at the Widom line of the WAIL simulation that is higher than the experimental value by a factor of three.

The temperature shift of the maxima between H_2O and D_2O of around 4 to 5 K, shown in Figs. 2D and 3, B and C, is similar to what has been observed as a constant shift in temperatures of the structural properties between the isotopes caused by nuclear quantum effects (*30*). Here we also observed that the position of the LLCP shifted to higher pressures for D_2O than for H_2O, which should also have its origin in nuclear quantum effects. This difference can partly explain why several molecular dynamics force fields (*25*, *31*–*33*) yielded maxima of κ_T that were too low at ambient pressure and pressure that was too high for the LLCP, because, in most cases, nuclear quantum effects were explicitly not taken into account and can increase for a pure classical liquid by a factor much larger than the difference in κ_T between H_2O and D_2O (*34*). We note that the size range of the fluctuating structural regions at the Widom line of around 2 nm requires large simulation boxes to capture the observed κ_T and ξ and currently limits the applicability of studying supercooled water both in nanosized droplets and confinements as a model system for bulk water.

Although the Widom line is defined on the basis of the maximum in ξ, other response functions can have lines of maxima as well. These lines may not overlap in temperature and only converge at the critical point, as observed in simulations around the liquid-gas critical point (*35*). In that case, there is quite a large difference in the maxima position of κ_T and C_P, which is not surprising because the two properties represent density and entropy fluctuations, respectively. However, here we observed that the position of maxima of ξ and κ_T almost exactly coincide, which is consistent with ξ being related to the length scales and κ_T reflecting the amount of density fluctuations. However, it is expected that the population of tetrahedral structures reaches 50%, which is the fraction at which the liquid structure undergoes the strongest change close to the Widom line (*36*–*38*), in accordance with the observations in Fig. 2D.

Figure 4B shows a schematic illustration of our findings in terms of density fluctuations. We have observed, in total, eight temperature-dependent maxima measurements—intensity of the structure factor in the low-q region, temperature derivative of the first diffraction peak, correlation length, and isothermal compressibility for both H_2O and D_2O at low pressure. These results demonstrate the existence of a Widom line where the fluctuations between low- and high-density liquid regions (*1*, *5*) become similar in population and maximized in terms of their length scale. The existence of the Widom line explains the diverging properties of supercooled water originating from an LLCP at moderately higher pressures with the isotope dependence indicative of the presence of nuclear quantum effects. The temperature of the Widom line is shifted between the two isotopes and is 229.2 ± 1 K for H_2O and 233.0 ± 1 K for D_2O at almost 0 bar. The use of x-ray lasers with ultrafast probing of liquid states provides the ability to determine thermodynamic response functions, correlation functions, and structural changes before crystallization can occur, and this can be generalized to many supercooled liquids. This method could allow for the probing of bulk supercooled water all the way down to the glassy state (*26*), which, studied under pressure, may also unlock the capability for direct observation of the LLCP, where the SAXS signal should become extremely strong because of critical fluctuations.

REFERENCES AND NOTES

1. A. Nilsson, L. G. M. Pettersson, *Nat. Commun.* **6**, 8998 (2015).
2. C. Huang *et al.*, *J. Chem. Phys.* **133**, 134504 (2010).
3. R. J. Speedy, C. A. Angell, *J. Chem. Phys.* **65**, 851–858 (1976).
4. P. G. Debenedetti, *J. Phys. Condens. Matter* **15**, R1669–R1726 (2003).
5. O. Mishima, H. E. Stanley, *Nature* **396**, 329–335 (1998).
6. F. Mallamace, C. Corsaro, H. E. Stanley, *Proc. Natl. Acad. Sci. U.S.A.* **110**, 4899–4904 (2013).
7. J. C. Palmer *et al.*, *Nature* **510**, 385–388 (2014).
8. P. H. Poole, F. Sciortino, U. Essmann, H. E. Stanley, *Nature* **360**, 324–328 (1992).
9. V. Holten, M. A. Anisimov, *Sci. Rep.* **2**, 713 (2012).
10. L. Xu *et al.*, *Proc. Natl. Acad. Sci. U.S.A.* **102**, 16558–16562 (2005).
11. S. Sastry, P. G. Debenedetti, F. Sciortino, H. E. Stanley, *Phys. Rev. E Stat. Phys. Plasmas Fluids Relat. Interdiscip. Topics* **53**, 6144–6154 (1996).
12. C. A. Angell, *Science* **319**, 582–587 (2008).
13. F. Perakis *et al.*, *Proc. Natl. Acad. Sci. U.S.A.* **114**, 8193–8198 (2017).
14. D. T. Limmer, D. Chandler, *J. Chem. Phys.* **135**, 134503 (2011).
15. E. B. Moore, V. Molinero, *Nature* **479**, 506–508 (2011).
16. Details of the materials and methods and supporting analysis of the experimental and theoretical data are available as supplementary materials.
17. J. A. Sellberg *et al.*, *Nature* **510**, 381–384 (2014).
18. D. Schlesinger, J. A. Sellberg, A. Nilsson, L. G. M. Pettersson, *J. Chem. Phys.* **144**, 124502 (2016).
19. L. B. Skinner, C. J. Benmore, J. C. Neuefeind, J. B. Parise, *J. Chem. Phys.* **141**, 214507 (2014).
20. R. W. Hendricks, P. G. Mardon, L. B. Shaffer, *J. Chem. Phys.* **61**, 319–322 (1974).
21. K. Amann-Winkel *et al.*, *Chem. Rev.* **116**, 7570–7589 (2016).
22. H. E. Stanley, *Introduction to Phase Transitions and Critical Phenomena* (Oxford Univ. Press, 1971).
23. C. Huang *et al.*, *Proc. Natl. Acad. Sci. U.S.A.* **106**, 15214–15218 (2009).

24. H. Kanno, C. A. Angell, *J. Chem. Phys.* **70**, 4008–4016 (1979).
25. H. Pathak *et al.*, *J. Chem. Phys.* **145**, 134507 (2016).
26. Y. Xu, N. G. Petrik, R. S. Smith, B. D. Kay, G. A. Kimmel, *Proc. Natl. Acad. Sci. U.S.A.* **113**, 14921–14925 (2016).
27. K. Stokely, M. G. Mazza, H. E. Stanley, G. Franzese, *Proc. Natl. Acad. Sci. U.S.A.* **107**, 1301–1306 (2010).
28. L.-P. Wang *et al.*, *J. Phys. Chem. B* **117**, 9956–9972 (2013).
29. Y. Li, J. Li, F. Wang, *Proc. Natl. Acad. Sci. U.S.A.* **110**, 12209–12212 (2013).
30. K. H. Kim *et al.*, *Phys. Rev. Lett.* **119**, 075502 (2017).
31. Y. Ni, J. L. Skinner, *J. Chem. Phys.* **144**, 214501 (2016).
32. S. K. Reddy *et al.*, *J. Chem. Phys.* **145**, 194504 (2016).
33. R. S. Singh, J. W. Biddle, P. G. Debenedetti, M. A. Anisimov, *J. Chem. Phys.* **144**, 144504 (2016).
34. M. Ceriotti *et al.*, *Chem. Rev.* **116**, 7529–7550 (2016).
35. P. Gallo, D. Corradini, M. Rovere, *Nat. Commun.* **5**, 5806 (2014).
36. F. Mallamace, *Proc. Natl. Acad. Sci. U.S.A.* **106**, 15097–15098 (2009).
37. J. Russo, H. Tanaka, *Nat. Commun.* **5**, 3556 (2014).
38. K. T. Wikfeldt, A. Nilsson, L. G. M. Pettersson, *Phys. Chem. Chem. Phys.* **13**, 19918–19924 (2011).

ACKNOWLEDGMENTS

This work has been supported by a European Research Council Advanced Grant under project no. 667205 and the Swedish National Research Council. The experiments were performed at beamline NCI of PAL-XFEL (proposal no. 2017-1st-CXI-006) funded by the Ministry of Science and ICT of Korea and at beamline BL3 of SACLA, with the approval of the Japan Synchrotron Radiation Research Institute (proposal no. 2015A8038). We thank L.-P. Wang for providing iAMOEBA compressibility data. The experimental data are available in the supplementary materials.

SUPPLEMENTARY MATERIALS

www.sciencemag.org/content/358/6370/1589/suppl/DC1
Materials and Methods
Supplementary Text
Figs. S1 to S18
Tables S1 to S6
References (*39*–*50*)

30 August 2017; accepted 2 November 2017
10.1126/science.aap8269

Science

Maxima in the thermodynamic response and correlation functions of deeply supercooled water

Kyung Hwan Kim, Alexander Späh, Harshad Pathak, Fivos Perakis, Daniel Mariedahl, Katrin Amann-Winkel, Jonas A. Sellberg, Jae Hyuk Lee, Sangsoo Kim, Jaehyun Park, Ki Hyun Nam, Tetsuo Katayama and Anders Nilsson

Science **358** (6370), 1589-1593.
DOI: 10.1126/science.aap8269

Pointing to a second critical point

One explanation for the divergence of many of the thermodynamic properties of water is that there is a critical point in deeply supercooled water at some positive pressure. For bulk water samples, these conditions are described as "no man's land," because ice nucleates before such temperatures can be reached. Kim *et al.* used femtosecond x-ray laser pulses to probe micrometer-sized water droplets cooled to 227 K (see the Perspective by Gallo and Stanley). The temperature dependence of the isothermal compressibility and correlation length extracted from x-ray scattering functions showed maxima at 229 K for H_2O and 233 K for D_2O, rather than diverging to infinity. These results point to the existence of the Widom line, a locus of maximum correlation lengths emanating from a critical point in the supercooled regime.

Science, this issue p. 1589; see also p. 1543

Science (print ISSN 0036-8075; online ISSN 1095-9203) is published by the American Association for the Advancement of Science, 1200 New York Avenue NW, Washington, DC 20005.